Journal of Alloys and Compounds 501 (2010) 333–338

Contents lists available at ScienceDirect

Journal of Alloys and Compounds

journal homepage: www.elsevier.com/locate/jallcom

Growth, structure and photocatalytic properties of hierarchical Cu–Ti–O nanotube arrays by anodization

Q. Ma [a], S.J. Liu [a,b,*], L.Q. Weng [a], Y. Liu [b], B. Liu [b]

[a] Materials Science and Engineering Division, Shenzhen Graduate School, Harbin Institute of Technology, Shenzhen, 518055, China
[b] State Key Laboratory for Powder Metallurgy, Central South University, Changsha 410083, China

ARTICLE INFO

Article history:
Received 12 January 2010
Received in revised form 10 April 2010
Accepted 15 April 2010
Available online 22 April 2010

Keywords:
Hierarchical nanotube
Cu–Ti alloy
Anodization
Dopant
Photocatalyst

ABSTRACT

Recently p-type Cu–Ti–O nanotubes have been explored in water-splitting photoelectrochemical pn-junction diodes to significantly improve the photoconversion efficiency. We reported on the growth and characterization of Cu–Ti–O nanotube arrays by anodizing directly Cu–Ti (30:70 wt%) alloy substrate. As-anodized hierarchical Cu–Ti–O nanotube arrays consist of two distinct Ti-rich and Cu-rich nanotube regions. It was found that mechanical stresses induced by copper doping resulted in the difference in the microstructure evolution of Cu-rich and Ti-rich regions. The oxygen vacancies induced by the high concentration Cu dopant into the Cu–Ti–O nanotube play a crucial role in determining the phase stabilization of anatase phase. The absorption edge of TiO_2 nanotube arrays was extended into the visible region by Cu doping. In degrading Methyl orange (MO), 21.2% MO was removed using Cu–Ti–O nanotube arrays after 240 min UV illumination. This result indicates the photocatalytic activity of Cu–Ti–O nanotube arrays to MO is reasonably high.

1. Introduction

Titania (TiO_2) is an important n-type semiconductor that exhibits excellent charge transfer properties and photochemical stability. The materials' architecture plays a critical role in optimizing the properties of the materials as well. Nanotube arrays could provide large surface area and uniform structure in the length, diameter, and wall thickness of the tubes. Highly ordered nanotubes could maintain well thermal and chemical stability in various environments [1]. Therefore, special attention has been paid to vertically aligned TiO_2 nanotube arrays due to the attracting properties and extensive applications in solar cells [2], photocatalysis [3], sensing devices [4], biomaterials [5], and drug delivery [6]. So far, various methods have been developed to fabricate highly ordered TiO_2 nanotube arrays, such as hydrothermal [7], template-assisted method [8], and electrochemical anodization [9]. The electrochemical anodization is considered as one of the most promising methods since long and vertical TiO_2 nanotube arrays could be easily fabricated by controlling the anodization voltage, time, and electrolyte. Among these, the electrolyte is a key factor that influences the structure and properties of as-synthesized TiO_2 nanotubes. The non-aqueous polar organic electrolyte, such as ethylene glycol electrolyte [10,11], formamide-based electrolyte [12,13], and dimethyl sulfoxide (DMSO) [14], exhibited some advantages over the aqueous electrolyte.

However, the wide bandgap of titania limits its activity to UV-radiation. Doping transition metals is an effective method to tailor and engineer the structure, phase, and bandgap. Copper is considered as one of the most suitable options since both cupric oxide (CuO, 1.2–1.5 eV bandgap) and cuprous oxide (Cu_2O, 2.0–2.2 eV bandgap) are p-type semiconductor with narrower bandgap. Moreover, it is low-cost, non-toxic, and relatively plentiful in resource. The copper-doped titanium oxide composite films were reported as photoelectrode and exhibited good photoelectrochemistry behavior [15]. Recently p-type Cu–Ti–O nanotube arrays have been fabricated as the self-biased heterojunction photoelectrochemical diodes for hydrogen generation [16].

In the present work, the substrate for the growth of Cu–Ti–O nanotube arrays is different from that in previous reports [2,17] where the Cu–Ti–O [2] and Ti–Fe–O [17] nanotube arrays were fabricated by anodizing Cu–Ti and Fe–Ti films on FTO coated glass, respectively. The hierarchical Cu–Ti–O nanotube arrays were prepared by anodizing Cu–Ti (30:70 wt%) alloy substrate directly. The growth, structure, and photocatalytic properties of nanotube arrays were investigated.

2. Materials and experimental procedure

Cu–Ti (30:70 wt%) alloy rod by Ar-arc melting was provided by the State Key Laboratory for powder metallurgy at Central South University, China. The Cu–Ti

* Corresponding author at: Materials Science and Engineering Division, Shenzhen Graduate School, Harbin Institute of Technology, Xili Shenzhen University Town, Shenzhen, Guangdong 518055, China.
Tel.: +86 755 26032046; fax: +86 755 26033504.
E-mail address: shaojunliu@gmail.com (S.J. Liu).

0925-8388/$ – see front matter © 2010 Elsevier B.V. All rights reserved.
doi:10.1016/j.jallcom.2010.04.099

alloy substrates were sliced from the Cu–Ti rod. Self-organized Cu–Ti–O nanotube arrays were grown by anodizing Cu–Ti alloy substrate. Ti foils (99.7% purity, 0.25 mm thick, Aldrich) were used as the substrate to grow undoped TiO_2 nanotubes. The substrates were first pretreated by polishing with silicon carbide abrasive paper and subsequently degreased by sonicating for 30 min in acetone and ethanol followed by rinsing with distilled water and drying in air. The anodization experiments were carried out in a formamide-based electrolyte comprising of 0.3 M NH_4F and 3 vol% deionized water at room temperature. The electrochemical anodization cell consisting of a two-electrode configuration with platinum as cathode and Cu–Ti substrate as anode was used to grow the nanotube arrays. The anodizing voltage was constant during the experiment. The as-anodized samples were carefully sonicated in distilled water for 15 s and then dried in air at 85 °C for 1 h. Crystallization of Cu–Ti–O nanotubes was attained by annealing at 450 °C for 2 h with 2 °C/min heating/cooling rate in pure oxygen.

The morphology and elemental analysis of the samples were characterized by a field emission scanning electron microscopy (Hitachi S-4700) equipped with an energy dispersive X-ray spectroscopy (EDS). The thickness of nanotube arrays was measured directly from the cross-sectional SEM images. The crystal structure was determined by X-ray diffractometer with thin film attachment (Rigaku, D/max 2500PC, Japan). The Raman spectra were measured by Renishaw Invia Micro-Raman Spectroscopy System using 514.5 nm Ar^+ blue laser as exciting source. The diffuse reflection spectra (DRS) were measured in the wavelength range of 250–800 nm using Shimadzu UV-2450 UV–vis spectrometer with $BaSO_4$ as a reference.

The photocatalytic activity experiments were carried out by degrading 20 mg l^{-1} methyl orange (MO) aqueous solution in a quartz curette with cooling water circulation system using 460W high-pressure UV light source. The photodegradation was interrupted at regular intervals (30 min, 60 min, 120 min, and 240 min, respectively) and a small amount of MO aqueous solution was taken out to analyze the degradation rate by spectrophotometer with absorbance wavelength of 463 nm. Since the MO concentration is linear with the absorbance of MO aqueous solution, the MO photocatalytic degradation percent was calculated using the following equation:

$$\eta = \frac{A_0 - A}{A_0} \quad (1)$$

where A_0 and A are the initial MO absorbance and the MO absorbance at time t, respectively.

3. Results and discussion

Fig. 1(a) shows SEM image of Cu–Ti alloy (30:70 wt%) substrate with two distinct areas, the dark and light gray area. EDS analysis indicates that the bright phases are Cu-rich with 1:2 Cu/Ti ratio (~34.3:65.7 at%). In contrast, the dark phases spotted and distributed in the matrix with size as large as 5–30 μm are Ti-rich consisting of 99.27 at% Ti and 1.73 at% Cu. Fig. 1(b) shows that two distinct regions become more obvious after anodizing. High magnification SEM images clearly show the significant difference in the morphology and microstructure between these two regions after anodization. As shown in Fig. 2(a), Cu-rich dark areas consist of the highly ordered Cu–Ti–O nanotube arrays with ~200 nm length, ~30 nm inner diameter, and ~10 nm wall thickness. Ti-rich areas consist of longer nanotubes with ~500 nm length, ~50 nm inner diameter, and ~10 nm wall thickness, as shown in Fig. 2(b). Undoped TiO_2 nanotube is grown to contrast its structure to that of Cu–Ti–O nanotube. Fig. 2(c) shows that undoped TiO_2 nanotube arrays prepared by anodizing pure Ti foil under the same conditions have >10 μm length, ~50 nm inner diameter, and ~10 nm wall thickness. It is observed that the nanotube gown on Cu-rich phase is much shorter than that grown on Ti-rich phase. It is expectable since the chemical dissolution of Cu-rich is much faster than that of Ti-rich in formamide-based electrolyte. Similar phenomena often were observed in anodizing Ti alloys where there are two phases or multiphases [18]. Insets in Fig. 2 are the cross-sectional SEM images. Fig. 3 shows that the structure of nanotubes annealed at 450 °C for 2 h is still stable and not destroyed. However, the structure breaks down when the annealing temperature further increases.

It is interesting to observe that the highly ordered Cu–Ti–O nanotube arrays are grown from Cu-rich regions near the Cu-rich and Ti-rich phase boundary (see Fig. 2(a)) while Ti-rich regions near the phase boundary consist of disordered TiO_2 nanotube arrays (see Fig. 2(b)). Evidently, the morphology of Cu–Ti–O nanotube is very sensitive to Cu concentration in the alloy substrate. It is

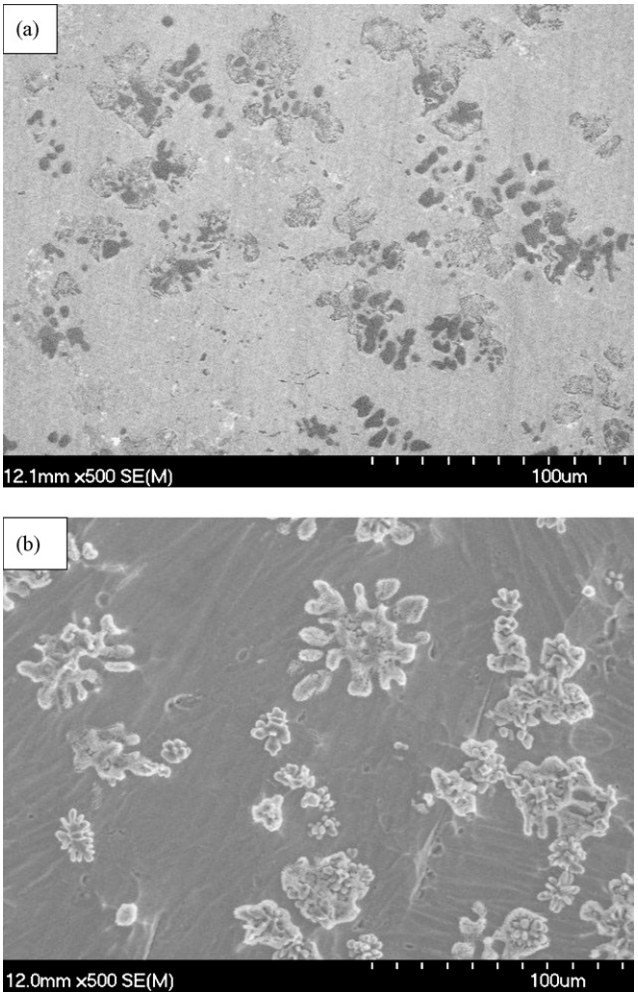

Fig. 1. SEM images of $Ti_{70}Cu_{30}$ alloy substrate (30:70 wt%): (a) before and (b) after anodizing.

generally believed there are two competing electric field assisted processes during the formation of TiO_2 nanotubes in F^- containing electrolytes. The first process involves the active dissolution of Ti metal to form a passive oxide layer and the second process is related to the chemical dissolution of the newly formed oxide [19,20]. The native TiO_2 lay is formed by the anodization of Ti layer in an acidic electrolyte under constant voltage. When ions diffuse inwards through the oxide layer at the interface between titanium and its native oxide layer, TiO_2 layer is dissolved at its outer interface with the acid. Due to the variation in the film roughness, the nanopores are formed across the surface of the TiO_2 and Ti–Cu–O layers where the enhanced local electric field exists, as shown in Fig. 4(a) and Fig. 5(a). There is an abrupt transition from nanopores to nanotubes with the continuous growth of nanopores into the oxide layer, as shown in Fig. 4(b). While the mechanism for the appearance of this transition is still not well established [20], this study is beyond our topic in the present paper. After the transition from nanopores to nanotubes is completed on both sides, the nanotubes continue to grow until the equilibrium thickness is established. The microstructure evolution of anodized TiO_2 nanotubes has been widely investigated [19–21], but in the present work we focus on the influence of Cu dopant on the microstructure evolution by anodizing Cu–Ti alloy substrate with two distinct phases. The microstructure evolution of the nanotube arrays near the phase boundary is shown schematically in Fig. 4(b)–(d) and the corresponding SEM images are shown in Fig. 5(b)–(d), respectively.

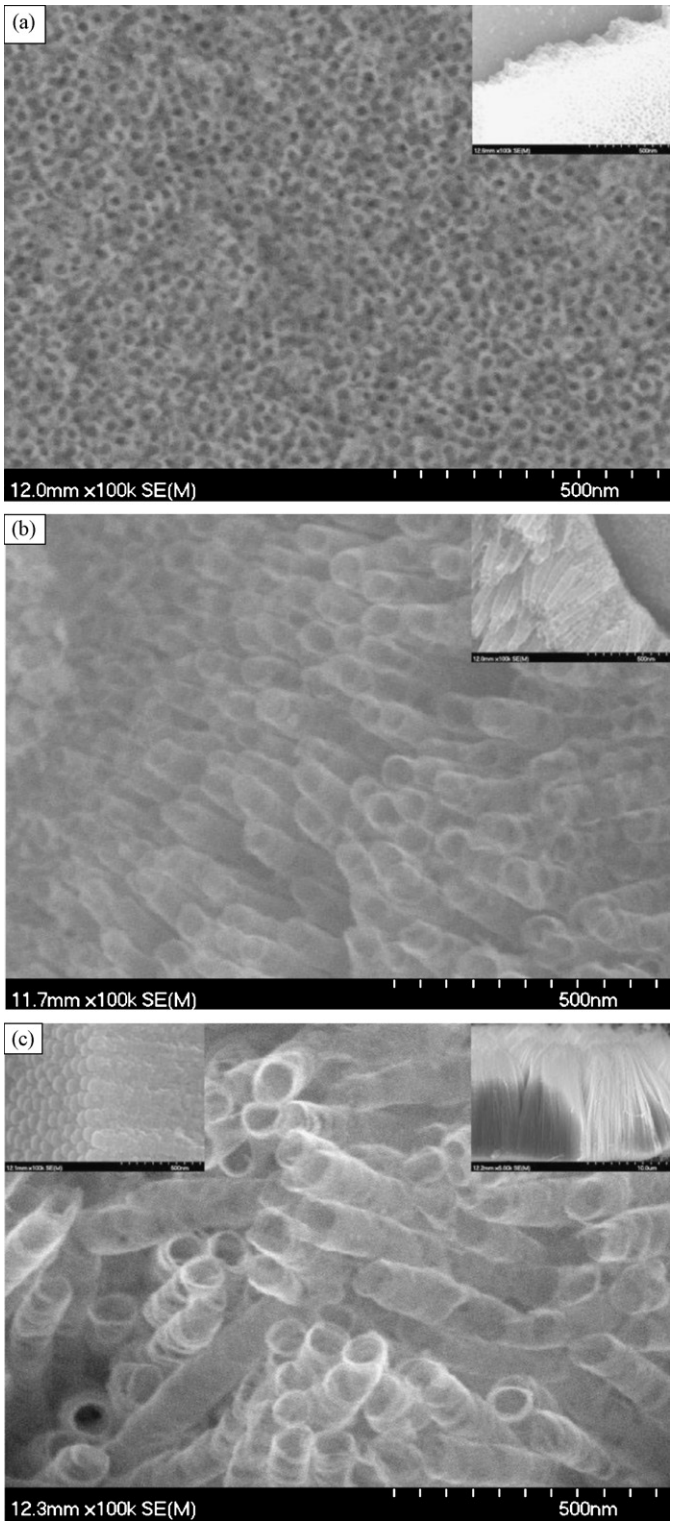

Fig. 2. Top-view and cross-section SEM images of highly ordered as-anodized nanotube arrays grown from the (a) Cu-rich phase, (b)Ti-rich phase, and (c) pure Ti foil.

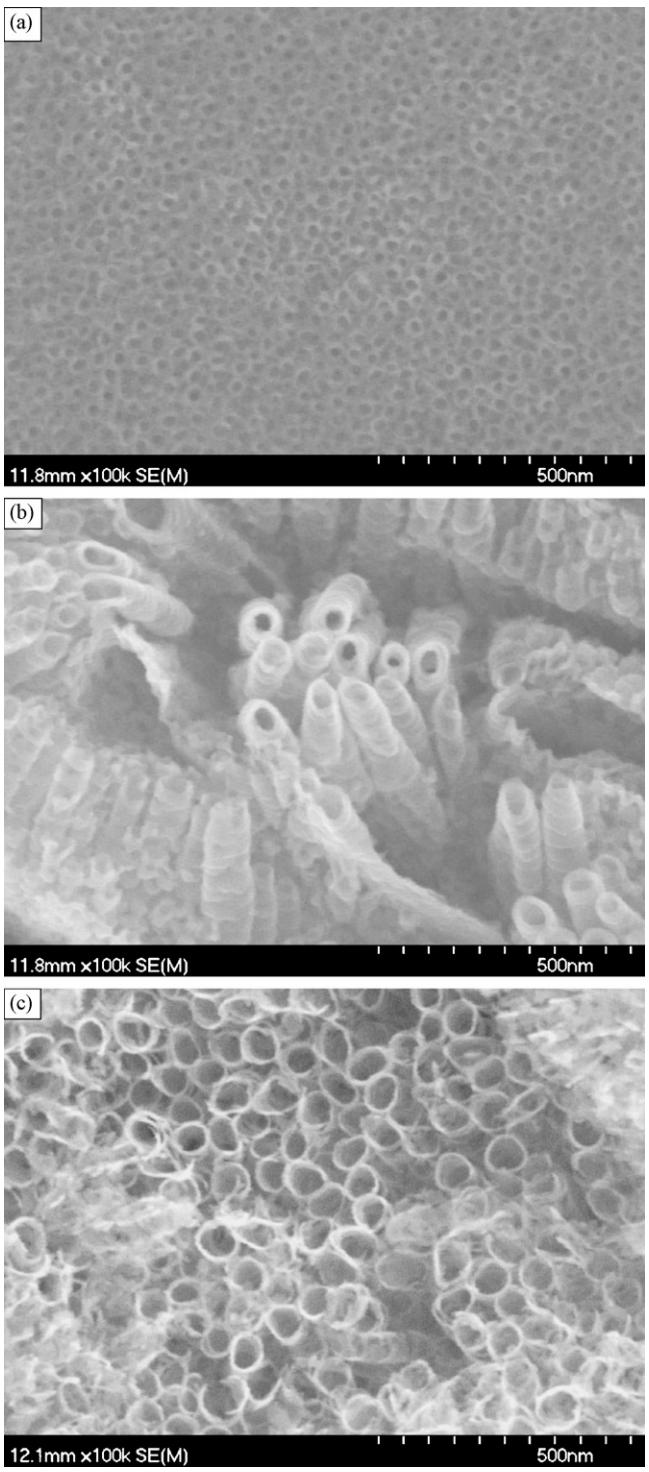

Fig. 3. Top-view SEM images of annealed samples grown from the (a) Cu-rich phase, (b) Ti-rich phase, and (c) pure Ti foil.

Since there is the largest difference in the chemical composition near the phase boundary, we focus our observation on these areas. In addition to the faster chemical dissolution of Cu-rich phase than that of Ti-rich phases, it should be mentioned that the density and style of point defect induced by the different Cu concentration might play a role in resulting in much shorter nanotube grown from Cu-rich phases. It is generally admitted that the large variation of volume expansion efficient, thickness, and point defect density in both sides of the phase boundary results in the existence of mechanical stress that becomes largest near the phase boundary [20]. We believe this mechanical stress is induced immediately at the beginning of the anodization. If the very small size of Ti-rich phase (5–30 μm) is considered, the mechanical stress near the phase boundary can be transferred effectively to the inside of nanotubes. Therefore, the appearance of the disordered TiO_2 nanotube arrays is hypothesized to be a result of mechanical stress at the

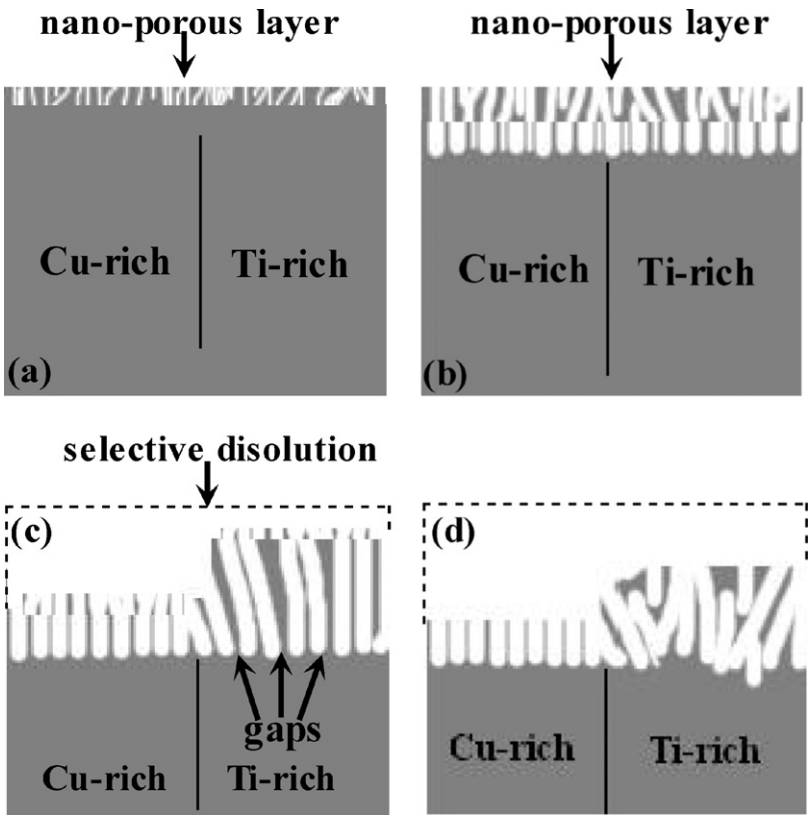

Fig. 4. Schematic diagram illustrating the microstructure evolution for nanotube arrays grown from Ti-rich and Cu-rich phases near the phase boundary, respectively.

Cu-rich/Ti-rich phase boundary. This disordering is especially obvious for the longer Ti-rich nanotubes nearby the phase boundary, as shown in Fig. 5(d).

Fig. 6 shows the XRD patterns of nanotube arrays grown on Cu–Ti alloy substrate and pure Ti foil and subsequently annealed at 450 °C in oxygen for 2 h. The diffraction peak of $2\theta \sim 40^\circ$ is ascribed to $CuTi_2$ on the substrate. In addition to the anatase diffraction peaks, weak diffraction peaks of $2\theta \sim 25.5^\circ$ and $2\theta \sim 38.5^\circ$ are assigned to rutile and CuO, respectively. It is noticeable that we do not observe the appearance of the rutile diffraction peaks of nan-

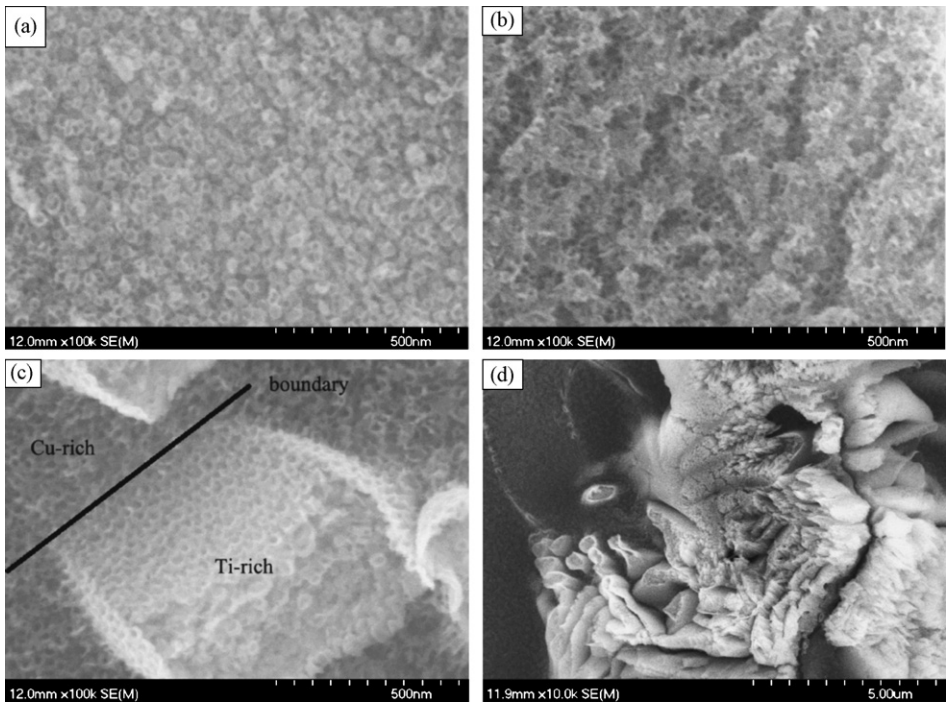

Fig. 5. SEM images corresponding to Fig. 4(a)–(d) and showing the microstructure evolution for nanotube arrays grown from Ti-rich and Cu-rich phases near the phase boundary.

otubes grown from pure Ti foils. While XRD usually gives average structural information and it is difficult for XRD to definitely distinguish the case where the minor Ti-rich phases coexist with the major Cu-rich phases, Raman spectroscopy is further used to detect the phase structure of the hierarchical nanotube arrays since it is a local probe tool and sensitive to the crystal structure and crystallinity of TiO_2. Fig. 7 shows Raman spectra of nanotubes grown on pure Ti foil, Ti-rich phase, and Cu-rich phase annealed at 450 °C for 2 h. Typical anatase Raman-active modes centered at ~146 cm^{-1}, ~199 cm^{-1}, ~397 cm^{-1}, ~517 cm^{-1}, and ~636 cm^{-1} are clearly observed for three types of nanotubes. Since the low frequency Raman mode centered at ~146 cm^{-1} represents the O–Ti–O mode that is very sensitive to the atomic ordering [22], obvious shift of Raman mode at ~146 cm^{-1} indicates that the Cu–Ti–O solid solution is formed by incorporation of Cu into Ti sites accompanying with the introduction of local disorder in titania. Two additional weak peaks centered at 248 cm^{-1} and 437 cm^{-1} corresponding to the rutile Raman-active modes, respectively, are easily observed in Cu-rich nanotube arrays.

It is generally anticipated that Cu dopants preferentially incorporating Ti site into titania are considered as point defects of acceptor nature since the valence of Cu ions (Cu^{2+} or Cu^{+}) is lower than that of Ti^{4+} ions. However, previous report by Grimes group showed [16] that Cu-doped TiO_2 nanotubes could behave as n-type or p-type semiconductor oxide depending on the Cu doping concentration. Therefore, the behavior of point defects introduced by Cu doping is much more complicated. It was reported that the anodized TiO_2 nanotubes doped with low Cu concentration are n-type semiconductor [16]. In this case, it behaves as the interstitial point defects with donor nature that help to stabilize the anatase phase. Additionally, the initial particle size plays a crucial important role in the anatase–rutile phase transformation that is related to the surface energy. However, this factor can be ruled out since there is almost no difference in the wall thickness among the Ti-rich, Cu-rich, and undoped TiO_2 nanotubes. On the other side, it was proposed that in the nano-sized TiO_2 particle the anatase to rutile phase transformation starts from the surface of the bulk anatase or from the interfaces between the anatase particles in the agglomerated TiO_2 particles [23]. The fresh transformed rutile grows at the expense of neighboring anatase particles. In our study, the case is different since the as-anodized nanotubes are almost isolated from each other. XRD results have shown that the excess CuO appears in the Cu-rich TiO_2 nanotubes. It is most likely that they are covering the surface of the anatase TiO_2. If it is assumed that the surface defect sites play an important role in the phase transformation, we expect that the excess CuO will easily occupy or deactivate the surface defect sites and retard the phase transformation. These observations lead us to conclude that Cu dopant is incorporated into Ti lattices and become substitutional point defects with acceptor nature in Cu-rich nanotubes. Subsequently, the oxygen vacancies are introduced to maintain the charge neutrality. Since oxygen vacancy is favorable to the high atomic mobility that promotes the phase transformation by the acceleration of atomic diffusion, the oxygen vacancy induced into the bulk region might play a dominant role during the anatase to rutile phase transformation.

DRS spectra of undoped TiO_2 and Cu–Ti–O nanotubes are shown in Fig. 8. The optical absorbing edge of undoped TiO_2 and Cu–Ti–O nanotubes is derived as 437 nm and 473 nm by dropping a line from the maximum slope of the curves to the *x*-axis, respectively [24]. As shown, there is an apparent absorption peak from ~400 nm to ~650 nm for the Cu–Ti–O nanotubes. As mentioned, CuO is p-type semiconductor with a bandgap ~1.7 eV corresponding to ~729 nm. The extra absorption edge in the Cu–Ti–O nanotubes spectra derived as ~727 nm is ascribed to the existence of CuO. The similar DRS spectrum was observed for TiO_2–Cu_2O composited

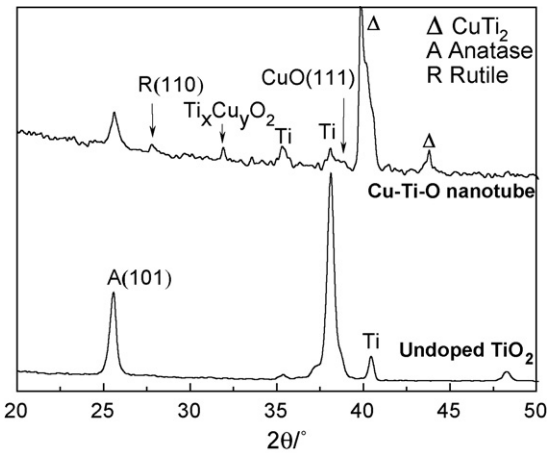

Fig. 6. XRD patterns of nanotube arrays grown from pure Ti foil and Cu–Ti alloy and annealed at 450 °C for 2 h in oxygen. Note: the intensity of XRD patterns for undoped TiO_2 has been divided by 10.

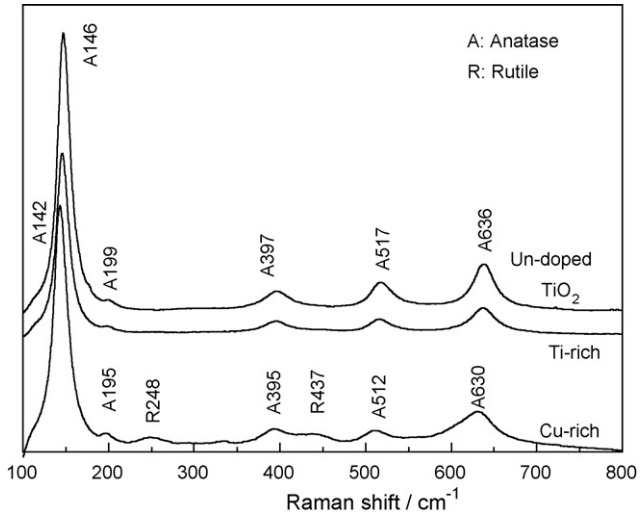

Fig. 7. Raman spectra of nanotube arrays grown from Cu-rich phases, Ti-rich phases in the alloy substrate, and pure Ti foils, respectively.

oxides [25]. Additionally, the DRS spectra for Cu–Ti–O nanotube arrays show a red shift into the visible region. While the UV–vis absorption band edge is a strong function of the crystallite size of nano-sized TiO_2 but the wall thickness of the TiO_2 and Cu–Ti–O nanotubes is almost the same, this phenomenon indicates that the reduced bandgap of undoped TiO_2 mainly results from the incorporation of a part of Cu dopants into titania.

Fig. 9 shows the photocatalytic degradation of MO with Cu–Ti–O nanotube arrays and undoped TiO_2 nanotube arrays. As shown, undoped TiO_2 nanotube arrays can degrade over 49.6% MO after 240 min UV illumination while only over 21.2% of MO is degraded by Cu–Ti–O nanotube arrays. There are several reasons that result in the lower photocatalytic efficiency of Cu–Ti–O nanotube arrays. Due to the faster chemical dissolution of Cu, the thickness of undoped TiO_2 nanotube arrays with ~10 μm is much larger than that of Cu–Ti–O nanotube arrays with ~500 nm under the same anodization condition. In addition to the larger surface area with more physically absorbed reactants on the inner and outer surfaces of the tubes, it was reported that the thickness of nanotube arrays significantly influenced the photocatalytic activity [26]. Zhuang et al. reported that the photocatalytic MO degradation of the TiO_2 nanotube arrays with 2.5 μm thickness is significantly higher than that of the ones with 400 nm thickness [26]. Moreover, as discussed

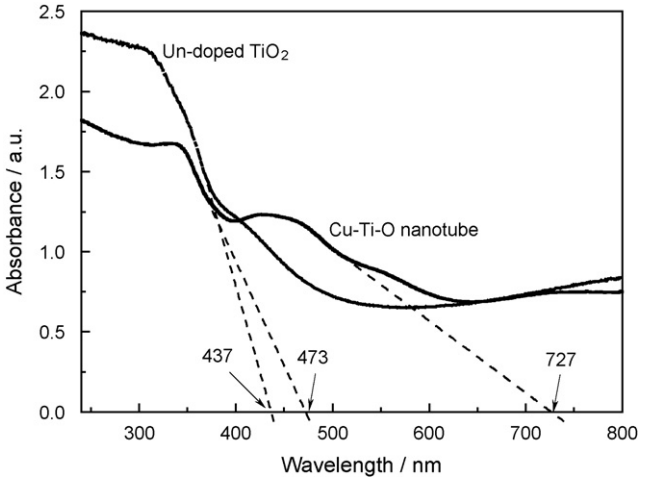

Fig. 8. DRS spectra of undoped TiO_2 and Cu–Ti–O nanotubes.

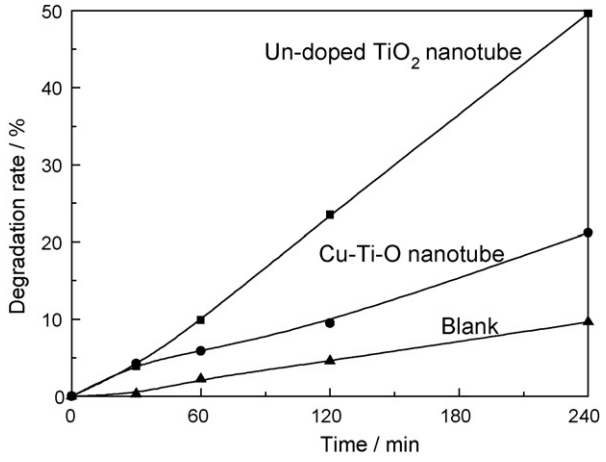

Fig. 9. Methyl orange photocatalytic degradation curves for undoped TiO_2 nanotube arrays and Cu–Ti–O nanotube arrays.

above, a part of anatase phase was transferred to rutile phase in Cu–Ti–O nanotube arrays and the photocatalytic activity of anatase is higher than that of rutile. However, it is interesting to notice that undoped TiO_2 nanotube array (~10 μm) is almost 20 times longer than Cu–Ti–O nanotube array (~500 nm). In contrast, the degradation rate of undoped TiO_2 nanotubes is only two times higher than that of Cu–Ti–O nanotubes. The normalized degradation rate in terms of the nanotube geometry for undoped TiO_2 and Cu–Ti array is derived as 4.96%/μm and 42.4%/μm, respectively. This results shows that the normalized degradation rate of Cu–Ti–O nanotube is much higher than that of undoped TiO_2. This value of Cu–Ti–O nanotube should be higher since Cu–Ti–O nanotube contains rutile phase and it is well known that the photocatalytic activity of anatase is higher than that of rutile. It was reported that the longer nanotube has a slower internal diffusion for reactants due to the capillarity [27], but these results show that Cu doping can be helpful to improve the degradation of MO. It is clear that further investigation separating the geometry and crystalline factor is needed to uncover the fundamental role of Cu doping on the photocatalytic activity of Cu–Ti–O nanotube arrays.

4. Conclusions

Hierarchical Cu–Ti–O nanotube arrays with two distinct Cu-rich and Ti-rich regions were fabricated by anodizing Cu–Ti (30:70 wt%) alloy. We grew the highly ordered Cu-rich Cu–Ti–O nanotube arrays and the disordered Ti-rich Cu–Ti–O nanotube bundles that are tapered conical from the Ti-rich and Cu-rich phases in the alloy substrate, respectively. Cu dopant was incorporated into Ti lattices in Cu-rich nanotubes and become substitutional point defects with acceptor nature. The oxygen vacancies induced by high concentration Cu dopant into the nanotube TiO_2 might play a dominant role in the phase stabilization of anatase phase. The absorption of TiO_2 nanotube arrays was extended into the visible region by Cu doping. It was found that 21.2% of MO was degraded by Cu–Ti–O nanotube arrays after 240 min UV illumination, indicating that the photocatalytic activity of Cu–Ti–O nanotube arrays to the decomposition of MO is reasonably high.

Acknowledgements

This work is supported by China National S & T Major Project through Grant Nos. 2009ZX07423-04, Shenzhen Fundamental Science Research Foundation through Nos. JC200903120193A, and State Key Laboratory of Powder Metallurgy Foundation at Central South University, Changsha, China.

References

[1] J.B. Chen, C.W. Wang, B.H. Ma, Y. Li, J. Wang, R.S. Guo, W.M. Liu, Thin Solid Films 517 (2009) 4390.
[2] K. Shankar, J. Bandara, M. Paulose, H. Wietasch, O.K. Varghese, G.K. Mor, T.J. Latempa, M. Thelakkat, C.A. Grimes, Nano Lett. 8 (2008) 1654.
[3] M. Zlamal, J.M. Macak, P. Schmuki, J. Krýsa, Electrochem. Commun. 9 (2007) 2822.
[4] O.K. Varghese, D.W. Gong, M. Paulose, K.G. Ong, C.A. Grimes, Sens. Actuators B: Chem. 93 (2003) 338.
[5] J. Park, S. Bauer, K.V.D. Mark, P. Schmuki, Nano Lett. 7 (2007) 1686.
[6] K.C. Popat, M. Eltgroth, T.J. LaTempa, C.A. Grimes, T.A. Desai, Biomaterials 28 (2007) 4880.
[7] T. Kubo, A. Nakahira, J. Phys. Chem. C 112 (2008) 1658.
[8] L.K. Tan, M.A.S. Chong, H. Gao, J. Phys. Chem. C 112 (2008) 69.
[9] H.E. Prakasam, K. Shankar, M. Paulose, O.K. Varghese, C.A. Grimes, J. Phys. Chem. C 111 (2007) 7253.
[10] M. Paulose, K. Shankar, S. Yoriya, H.E. Prakasam, O.K. Varghese, G.K. Mor, T.A. Latempa, A. Fitzgerald, C.A. Grimes, J. Phy. Chem. Lett. B 110 (2006) 16179.
[11] K. Shankar, G.K. Mor, H.E. Prakasam, O.K. Varghese, C.A. Grimes, Langmuir 23 (2007) 12445.
[12] F.F. Santiago, E.M. Barea, J. Bisquert, G.K. Mor, K. Shankar, C.A. Grimes, J. Am. Chem. Soc. 130 (2008) 11312.
[13] J.L. Tao, J.L. Zhao, X.X. Wang, Y. Kang, Y.X. Li, Electrochem. Commun. 10 (2008) 1161.
[14] S. Yoriya, M. Paulose, O.K. Varghese, G.K. Mor, C.A. Grimes, J. Phys. Chem. C 111 (2007) 13770.
[15] P. Xiao, B.B. Garcia, Q. Guo, D.W. Liu, G.Z. Cao, Electrochem. Commun. 9 (2007) 2441.
[16] G.K. Mor, O.K. Varghese, R.H.T. Wilke, S. Sharma, K. Shankar, T.J. Latempa, K.S. Choi, C.A. Grimes, Nano Lett. 8 (2008) 1906.
[17] G.K. Mor, H.E. Prakasam, O.K. Varghese, K. Shankar, C.A. Grimes, Nano Lett. 7 (2007) 2356.
[18] D.H. Kim, S. Fujimoto, P. Schmuki, H. Tsuchiya, Electrochem. Commun. 10 (2008) 910.
[19] C.A. Grimes, J. Mater. Chem. 17 (2007) 1451.
[20] G.A. Crawford, N. Chawla, Acta Mater. 60 (2009) 854.
[21] K. Yasuda, J.M. Macak, S. Berger, A. Ghicov, P. Schmuki, J. Electrochem. Soc. 154 (2007) C472.
[22] S.B. Aldabergenova, A. Ghicov, S. Albu, J.M. Macak, P. Schmuki, J. Non-Cryst. Solids 354 (2008) 2190.
[23] J.Y. Shi, J. Chen, Z.C. Feng, T. Chen, Y.X. Lian, X.L. Wang, C. Li, J. Phys. Chem. C 111 (2007) 693.
[24] G.K. Mor, O.K. Varghese, M. Paulose, K. Shanker, C.A. Grimes, Sol. Energy Mater. Sol. Cells 90 (2006) 2011.
[25] C.H. Han, Z.Y. Li, J.Y. Shen, J. Hazard. Mater. 168 (2009) 215.
[26] H.F. Zhuang, C.J. Lin, Y.K. Lai, L. Sun, J. Li, Environ. Sci. Technol. 41 (2007) 4735.
[27] H.C. Liang, Z.Z. Li, J. Hazard. Mater. 162 (2009) 1415.